

A Computational Investigation into the Combustion Byproducts of a Liquid Monopropellant

Mark E. Fuller^a, Richard H. West^b, C. Franklin Goldsmith^{a,*}

^aSchool of Engineering, Brown University, Providence, RI, 02912, USA

^bDepartment of Chemical Engineering, Northeastern University, Boston, MA 02115, USA

Abstract

A detailed chemical kinetic mechanism is developed for the gas-phase combustion of a liquid monopropellant, which is a blend of propylene-glycol-dinitrate, dibutyl-sebacate, and 2-nitro-diphenylamine (Otto Fuel II). The combustor is modeled as a steady-state burner-stabilized flame. The simulations reveal that not all of the dibutyl-sebacate is consumed in the flame, with approximately 5% persisting in the post-flame region. A large class of combustion byproducts are formed that have boiling points above the post-flame temperature and thus would be expected to condense out along the length of the combustor. This post-flame, two-phase behavior is hypothesized to be the cause of empirically observed oily build-up within the engine. This work represents a novel advancement in predictive modeling for propellant design, as it provides mechanistic insight into the possible origins of engine fouling.

Keywords:

Monopropellants, Nitrogen Chemistry, Automatic Mechanism Generation, Chemical Kinetics

1. Introduction

Air-independent propulsion presents a challenging engineering environment, particularly for thermal engines, since no ambient oxidizer is available as with terrestrial combustion engines. For the undersea environment, propulsion system selection is driven by operational requirements for energy and power density. Depending on these demands, unmanned vehicle propulsive systems have included, but are not limited to, energy storage in the form of bipropellant and monopropellant fuels[1–3]; combustion of metals[1, 3–5]; batteries, fuel cells, and semi-fuel cells[2, 6–9]; and environmental thermal energy harvesting[10]. The preceding propulsion systems can be designed to operate over several orders of magnitude of power and energy requirements; thermal engines with monopropellant fuels occupy a niche for power-dense applications at comparatively short run times. A commonly used liquid monopropellant is Otto Fuel II (OF), which consists of 76% (by mass) propylene-glycol-dinitrate (PGDN), 22.5% dibutyl-sebacate (DBS), and 1.5% 2-

nitro-diphenylamine (NDPA), where PGDN is the oxidizer, DBS is a plasticizer, and NDPA is added as a stabilizer. This particular blend was designed to provide a low vapor-pressure liquid that has sufficient energy density to provide the desired range but is safe to handle and store[11].

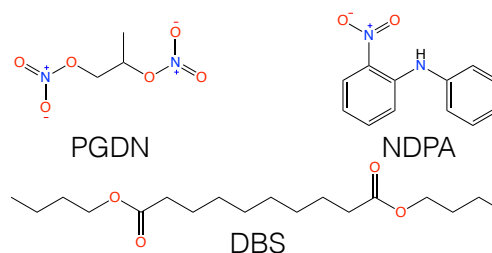


Figure 1: Chemical structures for the monopropellant.

However, OF does have undesirable consequences in operation. One particular problem is chemical fouling of the engine assembly. After each use, the combustor and engine are found to be coated in an oily carbonaceous residue, which, for lack of a more scientific term, will be referred to simply as *engine gunk*. The chemical nature of this residue, even its elemental composition, is not presently known. The presence of this gunk in-

*Corresponding author: C. Franklin Goldsmith
Email address: franklin_goldsmith@brown.edu (C. Franklin Goldsmith)

creases the cost of operation and the device downtime; furthermore, it represents a penalty on the overall efficiency of the system, since a non-trivial fraction of the monopropellant’s chemical energy is not converted into useful work. At present, it is not known whether the root cause of engine gunk can be traced to some aspect of engine design, engine operation, or is simply an unavoidable consequence of the chemical composition of OF.

Past work on OF and similar systems has not addressed these condensed combustion products and engine fouling. Early attempts to analytically model the combustion process were conducted with gas-phase equilibrium solvers that did not include condensed species[12]. More recent modeling work has continued to rely on outdated and simplified approaches assuming complete combustion to equilibrium gas-phase products[13].

Experimental work has also been conducted on this monopropellant and on the primary component, PGDN, but not in an operating engine which would allow for investigation of the fouling products. Experimental investigations, most notably by Faeth and coworkers, examined individual aspects of the fuel injection and combustion process in an attempt to characterize monopropellants for engineering applications. This has included examination of the evaporation individual droplets[14], measurement of bulk liquid fuel burning rates via strand burner[15] or in a pressurized chamber[16], and examination of the overall spray flame structure[17].

More recent work to develop an alternative monopropellant by Fontaine included a differential scanning calorimetry analysis of OF; this thesis represents the most recent known published work on its properties or behavior[18]. In summary, in nearly five decades of study, there has not been a detailed or conclusive investigation of the combustion products of OF and the mechanism by which fouling of the engine and gunk deposits occur. Further, in the decade since the work published by Fontaine, there have been significant advances in the modeling tools available, prompting a reexamination of this long-standing problem.

The aim of the present work is to develop a computational model for the combustion of OF under steady-state operation. The work combines electronic structure theory calculations on key species, automatic reaction mechanism generation, and simulations of a burner-stabilized flame. These results are combined with a thermochemical analysis of key product species, as a preliminary attempt to explain the origins of engine gunk.

2. Methods

2.1. Computational Chemistry

Density functional theory (DFT) calculations were performed for several key species and transition states. The M11/jun-cc-pVTZ functional/basis set was chosen for this system[19], based upon the authors’ prior experience with this functional for nitrogen compounds, as a suitable compromise between accuracy and feasibility for the size of these molecules[20].

Transition state theory (TST) calculations were performed for the decomposition of PGDN and its various products, as well as for NDPA and its products. Because these decomposition reactions involve a unimolecular intermediate, the rate constants will exhibit some degree of pressure dependence, and so microcanonical rate theory is needed to provide accurate temperature- and pressure-dependent rate constants. We used the RRKM/ME code MESS[21, 22], which is part of the computational kinetics package PAPP developed by Argonne National Laboratory[23]. A single exponential was used to model the collisional energy transfer, with $\langle \Delta E_{\text{down}} \rangle = 300 (T/298[\text{K}])^{0.85} \text{ cm}^{-1}$, based upon previous work for molecules of this size[24–26]. For transition states that have a first-order saddle point in potential energy, standard rigid-rotor harmonic-oscillator models were used to compute the microcanonical rate coefficients.

For the bond fission channels – such as the initial cleavage of the O–N bonds in PGDN and the C–N bond in NDPA – a simple analytic model was used to describe the interaction potential, as implemented using the PhaseSpaceTheory keyword in MESS[27–29]. For these barrierless reactions, the interaction potential between the two radicals is assumed to follow a simple αr^{-6} form, and the coefficient α was adjusted so that the high-pressure limit of the reverse reaction (*e.g.* $\text{R} + \text{NO}_2$) had a rate coefficient of approximately $3 \times 10^{-11} \text{ cm}^3/\text{molecule-s}$, which is a reasonable approximation to the radical + NO_2 reactions in the high-pressure limit[30, 31].

2.2. Mechanism Development

The elementary reaction mechanism for monopropellant combustion was generated using the open-source software RMG (version 2.1)[32, 33]. RMG represents chemical species using chemical graph theory, which allows for efficient methods for checking if a species is already present in a mechanism, and for decomposing the molecule into its functional groups. For many of the most common combustion intermediates, accurate thermodynamic properties are tabulated; for novel species,

these properties are estimated via group additivity[34]. Reactions are classified according to “reaction families”, which include templates to identify when a reaction can occur, a recipe to describe how the reaction changes the chemical graphs of the reactant(s), and rules to predict the Arrhenius parameters. RMG will consider every possible reaction that can be predicted from the reaction families, but it only includes those reactions that have a significant flux[35]. For a detailed description of RMG, the reader is referred to the recent work by Gao et al.[33].

In RMG, the reactor model used in the rate-based screening algorithm is an isothermal, isobaric batch reactor; multiple reactors with different initial conditions can be used to create a mechanism that is valid over a broad range of conditions. Unfortunately, generating a mechanism for a monopropellant flame isn’t quite so simple as providing the initial composition and a range of temperatures and pressures. Because the monopropellant is fuel-rich, some conditions will lead to the growth of heavier molecular weight compounds. Under these conditions, if the `terminationTime` is set too long, RMG will (correctly) continue to follow the paths with the highest flux until invariably the computer runs out of memory.

Preliminary modeling results suggest that the decomposition kinetics of the oxidizer (PGDN) and plasticizer (DBS) are largely decoupled. The oxidizer rapidly decomposes in the pre-flame regime, whereas the plasticizer undergoes a much slower pyrolysis and partial oxidation process in an atmosphere that is dominated by the PGDN decomposition products: NO_2 , NO , CH_2O , CH_3CHO , CH_3 , and H . This decoupling of the chemistry can be used to simplify the model generation process in a manner that captures the essential cross reactions but avoids excessive memory requirements. In this approach, RMG was run twice. In the first iteration, a single reactor was used, which contains the original propellant formulation at $T = 800$ K and $P = 10$ atm, with a `terminationConversion = 99%` conversion of PGDN. This reactor obtains the rapid decomposition of PGDN, as well as some of the lower-temperature cross reactions between the PGDN decomposition products and DBS and NPDA. Once this mechanism was complete, a second reactor was added to the input file. The input composition of the second reactor was set to the exit composition of the first reactor, and the temperature was increased to $T = 1600$ K, with a termination criterion of `terminationConversion = 99%` conversion of DBS. Effectively, the first reactor corresponds to the pre-flame region, and the second reactor corresponds to the post-flame region.

The high-pressure limit rate coefficients from Section 2.1 were added to a local RMG reaction library. To further reduce the complexity of the mechanism, the size of the products were limited. As will be demonstrated in Section 3, we need only include species up to 35 heavy atoms to demonstrate that some species will begin to condense out.

2.3. Flame Simulations

The open-source software package CANTERA was used to simulate the combustion chamber[36]. The combustor is approximated as a 1D burner stabilized flame[37]. The inlet stream is approximated to be a vapor that has been pre-heated to 400 K at 10 atm, with a mass flow rate of 0.1 kg/s. The profile was refined until there were 100 grid points over a range of 0.1 m. Pressure fluctuations associated with the sinusoidal dynamics of the valve assembly are assumed to be inconsequential for the model simulations.

3. Results

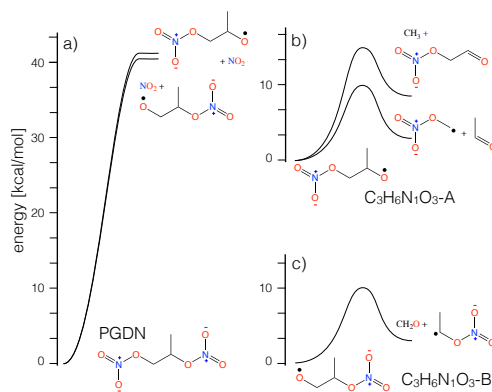


Figure 2: Potential energy diagram for propylene-glycol dinitrate (PGDN) and its primary thermal decomposition products. The HONO-elimination pathways are omitted from (a) for clarity but are included in Table 1. (b) and (c) illustrate the dominant beta-scission pathways for the products in (a).

The potential energy surface (PES) for the decomposition of PGDN at the M11/jun-cc-pVTZ level is shown in Figure 2a. The most significant decomposition pathways for PGDN are cleavage of the two $\text{O}-\text{NO}_2$ groups. Each of these decomposition pathways also has a corresponding HONO-elimination channel, but these pathways are omitted from Figure 2a, because those rate constants are roughly six orders of magnitude smaller. The insets Figure 2b-c correspond to the subsequent decomposition kinetics of these two oxy-radicals,

$C_3H_6N_1O_3$ -A and $C_3H_6N_1O_3$ -B, respectively. The decomposition product for $C_3H_6N_1O_3$ -A, CH_2ONO_2 , is not stable and immediately dissociates to $CH_2O + NO_2$. Similarly, the decomposition product for $C_3H_6N_1O_3$ -B, CH_3CHONO_2 , is not stable and immediately dissociates to $CH_3CHO + NO_2$. Thus, these two reactions were input into RMG via a custom library, even though they would not match any of RMG's reaction templates.

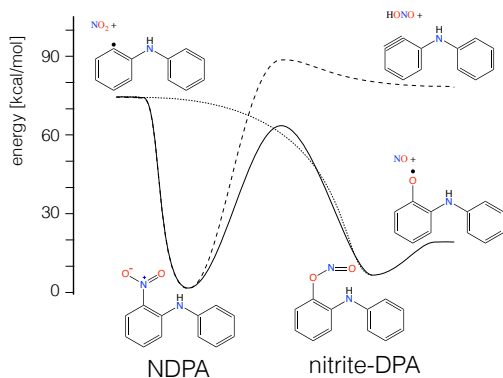


Figure 3: Potential energy diagram for 2-nitrodiphenylamine (NDPA).

The M11/jun-cc-pVTZ PES for NDPA is shown in Figure 3. The main decomposition product is the aminophenyl-benzyl + NO_2 , even though the transition state for nitro-nitrite isomerization is lower in energy. For the 2-nitrite-diphenylamine (lower right), the O-NO bond is so weak that this nitrite is not a stable species under conditions of interest and immediately dissociates to 2-phenylamine-phenoxy + NO. The aminophenyl-benzyl (upper left) undergoes a beta-scission to form benzyne + a resonantly stabilized phenyl-aminyl radical. It is also possible for the amine in NDPA to lose its hydrogen, resulting in a resonantly stabilized radical. However, this process is 20 kcal/mol more endothermic than the competing C- NO_2 cleavage and is omitted.

The rate coefficients evaluated at 10 atm are listed below in Table 1.

Table 1: Arrhenius parameters for selected rate constants, evaluated at 10 atm. Units are in cm^3 , mol, s, and kcal, with $T_{ref} = 1$ K for the temperature dependence of the pre-exponential factor.

Reaction	A	n	E_a	$k(1000\text{ K})$
$PGDN \rightleftharpoons C_3H_6N_1O_3-1 + NO_2$	4.3×10^{81}	-20.2	60.4	6.8×10^7
$PGDN \rightleftharpoons C_3H_6N_1O_3-2 + NO_2$	8.1×10^{83}	-20.9	62.2	4.1×10^8
$PGDN \rightleftharpoons C_3H_5N_1O_3-1 + HONO$	3.3×10^{77}	-20.8	64.0	1.3×10^1
$PGDN \rightleftharpoons C_3H_5N_1O_3-2 + HONO$	1.1×10^{76}	-20.6	63.5	2.3×10^1
$C_3H_6N_1O_3-1 \rightleftharpoons CH_2O + CH_3CHO + NO_2$	1.2×10^{31}	-6.2	14.0	2.6×10^9
$C_3H_6N_1O_3-2 \rightleftharpoons CH_3CHO + CH_2O + NO_2$	4.8×10^{31}	-6.4	14.4	2.2×10^9
$C_3H_6N_1O_3-2 \rightleftharpoons OCHCH_2ONO_2 + CH_3$	3.6×10^{32}	-6.9	17.2	1.3×10^9
$OCHCH_2ONO_2 \rightleftharpoons HCO + CH_2O + NO_2$	1.3×10^{62}	-14.4	52.1	3.4×10^6
$NDPA \rightleftharpoons C_{12}H_{10}N_1 + NO_2$	4.8×10^{63}	-14.9	87.6	7.3×10^6

The first stage of the RMG process generated 50 species and 184 reactions for the pre-flame regime; the final mechanism contained 547 species and 6191. Earlier versions of RMG were not able to converge with NPDA as a reactive species, because the presence of polyaromatic compounds like NDPA lead to numerical instabilities. However, a recent modification to RMG has vastly improved its ability to handle aromatic chemistry, and these improvements had a significant impact on the present work[38].

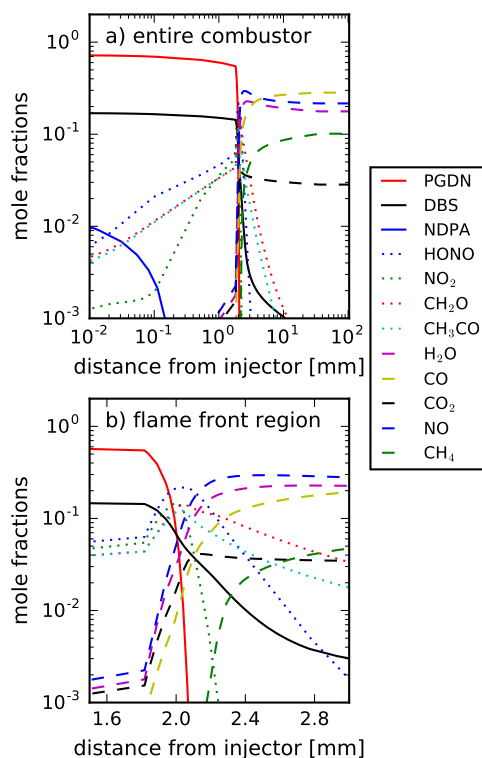


Figure 4: Mole fractions of major species along the length of the combustor. The three solid lines are the reactants in the monopropellant formulation. The dotted lines correspond to short-lived intermediates in the vicinity of the flame front. The dashed lines are the more stable combustion products. (a) represents the entire combustor length (logarithmic in x -coordinate), and (b) is an expansion (linear in x -coordinate) around the flame front.

The major chemical species from the burner simulations are presented in Figure 4. The profiles indicate that NDPA begins to decompose immediately, along with a steady decomposition of PGDN. The radical concentration reaches a tipping point at ~ 2 mm from injection, and the flame front represents a near step-change in the composition. The majority of the compounds present in the flame front are the decomposition products of PGDN: CH_2O , CH_3CHO , NO_2 , and HONO. Figure

4b zooms on on the flame front region, which is approximately 5-6 mm thick under these conditions. The majority of the HONO concentration within the flame front comes from H-abstraction and disproportionation, and not from the direct HONO-elimination from PDGN or NDPA. Immediately after the flame, incomplete combustion products – CO, NO, H₂O, and CH₄ – make up the majority of the gas composition. In the pre-flame region, DBS is largely unreactive, but approximately 95% of the DBS is combusted within the flame. A small fraction continues to crack downstream of the flame, producing a sizable concentration of smaller straight-chain species that have varying degrees of oxygenation and saturation.

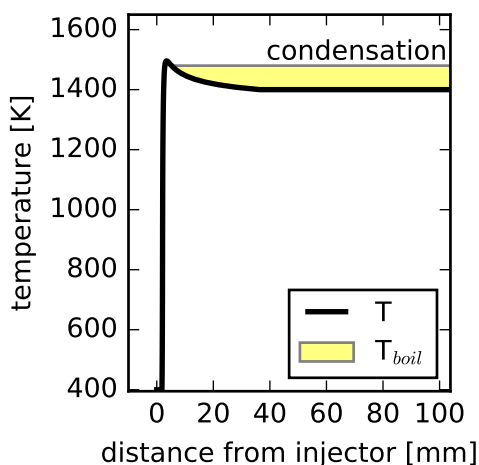


Figure 5: Temperature profile along the length of the combustor. The yellow shaded area denotes the post-flame region in which the vapor temperature may drop below the boiling point of many of the species.

Figure 5 presents the simulated temperature profile from the RMG mechanism. Because the monopropellant is so fuel-rich, the peak temperature is considerably lower than it would be for a stoichiometric mixture. The temperature peaks at 1495 K at 3 mm from the injector, and then decreases to 1410 K by 30 mm. The slight drop in temperature in the post-flame region is likely due to the continued decomposition of DBS and its products. The unimolecular decomposition of DBS and its subsequent products are endothermic, and the gradual fracturing of the $\sim 5\%$ of DBS that remains in the post-flame region leads to a modest cooling effect. The comparatively low temperature in the post-flame region, coupled with the low concentration of potential oxidizers, such as NO₂, suggest that these fragments will continue to pyrolyze rather than oxidize. This temperature decrease is particularly important, because it suggests that

the post-flame temperature may indeed drop below the boiling point for some of the compounds.

Our present working hypothesis is that various aromatic radicals react with the remaining DBS decomposition fragments and then condense out in the post-flame region. Of particular interest is the fate of two radicals, 2-phenylamine-phenoxy and phenyl-aminy, that are formed from the prompt dissociation of 2-nitrite-diphenylamine. Owing to their resonance stabilization, these radicals do not react with closed-shell species and are difficult to oxidize; instead, they recombine with other radicals – including themselves and straight-chain unsaturated radicals that result from the pyrolysis of DBS – to form heavier molecular weight compounds. As mentioned previously, we chose an upper limit of 35 heavy atoms for this process; otherwise, it becomes increasingly difficult to get the flame simulations to converge. By 35 heavy atoms, however, we can begin to make semi-quantitative predictions regarding the phase change behavior.

Although RMG cannot predict phase-change properties for all species automatically, we can estimate the thermodynamic properties for individual species “by hand” on a case-by-case basis as part of a post-processing routine. By using the method of Joback[39], we can approximate the boiling point T_{boil} and enthalpy of vaporization ΔH_{vap} at standard state for select species. The results were tested against various species that are structurally similar and are available through ACDLABS[40]. Overall, the agreement was typically within $\pm 20^\circ$ and ± 10 kJ/mol, respectively, which is sufficient for the present work. RMG already uses the Joback method to predict transport properties (*e.g.* Lennard-Jones σ and ϵ)[41], and future versions will implement the Joback method for vapor-liquid equilibrium (VLE) properties as well. Using the Clausius-Clapeyron equation, we can extrapolate the boiling point to higher pressures:

$$T_{\text{boil}}(P) = \left(\frac{1}{T_{\text{boil}}(1 \text{ bar})} - \frac{R}{\Delta H_{\text{vap}}} \ln \left[\frac{P}{1 \text{ bar}} \right] \right)^{-1} \quad (1)$$

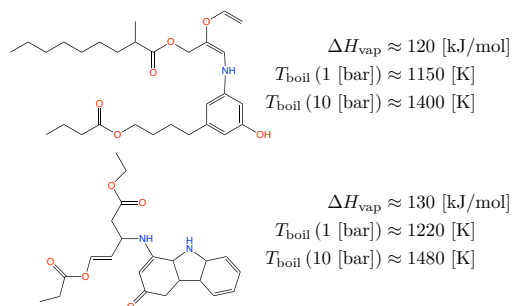


Figure 6: Two typical species that are predicted by RMG in the post-flame region, along with their estimated vapor-liquid equilibrium properties.

Figure 6 presents two typical molecules that are among the hundreds produced by RMG. The molecular structure of these two particular species and the reactions that produced them is not our primary objective. Rather, we wish to emphasize that RMG produces many structurally similar compounds that contain one or more phenyl-amine, alkane, alkene, ketone, and other functional groups, with a total of 30 or more heavy atoms. Application of the Joback method suggests that many of these species will have a boiling point greater than 1400 K at 10 bar. Automatically computing the boiling point is not yet possible within RMG, so we cannot estimate the phase-change properties for all species. A visual inspection of the results suggests that roughly 100 of the 547 species are qualitatively similar to those species in Figure 6. The boiling points of these species, and the reaction paths that form them, will be the subject of future investigation.

If we examine the flame profile in Figure 5, we note that boiling points for the two species in Figure 6 are above the post-flame temperature. This area is highlighted in yellow. Based upon these thermodynamic considerations, we expect that a fraction of the post-gas products will condense. The total concentration of these compounds is quite small – typically on the ppb level – but the condensation of these trace gas species could serve as nucleation sites for further agglomeration. Furthermore, the actual motor is actively cooled on the surface of the combustor, and this heat loss will further drop the post-flame temperature along the length of the combustion chamber, thereby encouraging the condensation of even more products.

Finally, it should be noted that these simulations were performed using the ideal-gas equation of state. Given the absence of N_2 or other diluents that have compressibility factors $Z \approx 1$ at $P \geq 10$ atm, it is quite possible that the vapor phase deviates significantly from real-gas behavior. If we assume that $P \sim 10$ atm is within the

compressibility well ($Z < 1.0$), then the real-gas post-flame temperature would be lower than the ideal gas prediction. This real-gas effect would further promote condensation. The PI is currently collaborating with Prof. Steven DeCaluwe (Colorado School of Mines) to implement real-gas equations of state in 1D burner flames for monopropellant combustors.

4. Conclusion

A detailed chemical kinetic mechanism is presented for a liquid monopropellant, Otto Fuel II. The mechanism was generated using the software RMG, and was further refined by computational quantum chemistry and theoretical kinetics calculations for the key reactions of the oxidizer. This mechanism was implemented in a model for a burner-stabilized flame. This approach represents the first computational examination of the combustion of Otto Fuel II. The model suggests that the temperature downstream of the flame front is insufficient to maintain a pure vapor phase. Some large molecular weight products, typically formed from the incomplete combustion of aromatic radicals, will condense in the post-flame region. It is hypothesized that these condensates are the chemical origin of oily residue that build up inside the engine housing. Application of automatic reaction mechanism generating software provides a methodology for understanding the observed engine fouling. As RMG becomes better at predicting nitrogen chemistry in general and nitrate esters in particular, it has the potential to become an indispensable design tool for novel propellants and combustor design. Future experimental work is needed to characterize the combustion byproducts, and future computational work is needed to quantify real gas effects and key kinetic pathways.

Acknowledgments

This work is supported by the U.S. Office of Naval Research through ONR Grant Number N00014-16-1-2769, with Dr. Maria Medeiros as the program manager. MEF gratefully acknowledges additional support from Brown University. RHW gratefully acknowledges support from Northeastern University. MEF and CFG would like to thank Dr. Joseph H. Fontaine, Christopher A. Matthews, and Raymond W. Roberts for many stimulating discussions, and Eric Tierney for early assistance with the electronic structure calculations.

References

- [1] L. Greiner (Ed.), *Underwater Missile Propulsion*, Compass Publications, Inc., 1967.
- [2] E. W. Jolie, A brief history of U.S. Navy torpedo development, Tech. Rep. TD 5436, Naval Underwater Systems Center (1978).
- [3] D. Kiely, Review of underwater thermal propulsion, in: 30th Joint Propulsion Conference and Exhibit, American Institute of Aeronautics and Astronautics, 1994.
- [4] J. N. Mattavi, F. E. Heffner, A. A. Miklos, *The Stirling Engine for Underwater Vehicle Applications*, SAE International, 1969.
- [5] T. Miller, J. Walter, D. Kiely, A next-generation AUV energy system based on aluminum-seawater combustion, in: Proceedings of the 2002 Workshop on Autonomous Underwater Vehicles, 2002., IEEE, 2002, pp. 111–119.
- [6] W. S. Wilcock, P. C. Kauffman, Development of a seawater battery for deep-water applications, *Journal of Power Sources* 66 (1-2) (1997) 71–75.
- [7] M. G. Medeiros, R. R. Bessette, C. M. Deschenes, C. J. Patrissi, L. G. Carreiro, S. P. Tucker, D. W. Atwater, Magnesium-solution phase catholyte semi-fuel cell for undersea vehicles, *Journal of Power Sources* 136 (2) (2004) 226–231.
- [8] Q. Cai, D. Brett, D. Browning, N. Brandon, A sizing-design methodology for hybrid fuel cell power systems and its application to an unmanned underwater vehicle, *Journal of Power Sources* 195 (19) (2010) 6559–6569.
- [9] A. Mendez, T. Leo, M. Herreros, Current state of technology of fuel cell power systems for autonomous underwater vehicles, *Energies* 7 (7) (2014) 4676–4693.
- [10] D. Webb, P. Simonetti, C. Jones, SLOCUM: an underwater glider propelled by environmental energy, *IEEE Journal of Oceanic Engineering* 26 (4) (2001) 447–452.
- [11] O. Reitlinger, Liquid monopropellants of reduced shock sensitivity and explodability, U.S. Patent 4026739 (1963).
- [12] L. Bisci, Analytical study to determine the Otto Fuel Composition II combustion products, in: AIAA Second Annual Meeting, 1965.
- [13] J. Bai, J. jun Dang, Numerical simulation for turbulent combustion in underwater vehicle combustor, *Procedia Engineering* 31 (2012) 844–849.
- [14] G. M. Faeth, Prediction of pure monopropellant droplet life histories, *AIAA Journal* 8 (1970) 1308–1314.
- [15] G. Faeth, High-pressure liquid-monopropellant strand combustion, *Combustion and Flame* 18 (1) (1972) 103–113.
- [16] W. F. McBratney, Windowed chamber investigation of the burning rate of liquid monopropellants for guns, Memorandum Report ARBRL-MR-03018, U.S. Army Armament Research and Development Command (1980).
- [17] G. M. Faeth, T. W. Lee, M. E. Kounalakis, L. K. Tsang, Structure of monopropellant spray flames at elevated pressures, Final Report GDL/GMF-90-01, U.S. Army Research Office (1990).
- [18] J. H. Fontaine, Development of a novel hydroxyl ammonium nitrate based liquid propellant for air-independent propulsion, Ph.D. Thesis, Brown University (2006).
- [19] R. Peverati, D. G. Truhlar, Improving the Accuracy of Hybrid Meta-GGA Density Functionals by Range Separation, *Journal of Physical Chemistry Letters* 2 (2011) 2810–2817.
- [20] J. Chai, C. F. Goldsmith, Rate coefficients for fuel + NO₂: Predictive kinetics for HONO and HNO₂ formation, *Proceedings of the Combustion Institute* 36 (2017) 617–626.
- [21] Y. Georgievskii, J. A. Miller, M. P. Burke, S. J. Klippenstein, Reformulation and solution of the master equation for multiple-well chemical reactions, *The Journal of Physical Chemistry A* 117 (46) (2013) 12146–12154.
- [22] Y. Georgievskii, S. J. Klippenstein, MESS: Master equation system solver 2016.3.23, <http://tcg.cse.anl.gov/papr/codes/mess.html/>.
- [23] Y. Georgievskii, J. A. Miller, M. P. Burke, S. J. Klippenstein, PAPER: Predictive automated phenomenological rates v1, <http://tcg.cse.anl.gov/papr/>.
- [24] C. F. Goldsmith, W. H. Green, S. J. Klippenstein, Role of O₂ + QOOH in low-temperature ignition of propane. 1. Temperature and pressure dependent rate coefficients, *The Journal of Physical Chemistry A* 116 (13) (2012) 3325–3346.
- [25] C. J. Annesley, C. F. Goldsmith, R. S. Tranter, A shock tube laser schlieren study of methyl acetate dissociation in the fall-off regime, *Physical Chemistry Chemical Physics* 16 (2014) 7241–7250.
- [26] C. J. Annesley, J. B. Randazzo, S. J. Klippenstein, L. B. Harding, A. W. Jasper, Y. Georgievskii, B. Ruscic, R. S. Tranter, Thermal dissociation and roaming isomerization of nitromethane: Experiment and theory, *The Journal of Physical Chemistry A* 119 (28) (2015) 7872–7893.
- [27] J. O. Hirschfelder, E. Wigner, Some quantum-mechanical considerations in the theory of reactions involving an activation energy, *Journal of Chemical Physics* 7 (1939) 616.
- [28] W. H. Miller, Unified statistical model for “complex” and “direct” reaction mechanisms, *Journal of Chemical Physics* 65 (1976) 2216–2223.
- [29] W. J. Chesnavich, L. Bass, T. Su, M. T. Bowers, Multiple transition states in unimolecular reactions: A transition state switching model. application to the C₄H₈ + · system, *Journal of Chemical Physics* 74 (1981) 2228–2246.
- [30] X. Chen, C. F. Goldsmith, Theoretical predictions for the unimolecular decomposition of RDX, *Proceedings of the Combustion Institute* 37 (2017) (submitted).
- [31] J. B. Randazzo, M. E. Fuller, A. W. Jasper, C. F. Goldsmith, R. S. Tranter, Experimental investigations of the thermal dissociation of n-propyl, n-butyl, and iso-butyl nitrites, *Proceedings of the Combustion Institute* 37 (2017) (submitted).
- [32] R. H. W. William H. Green, Reaction mechanism generator, version 2.1.0. URL <http://rmg.mit.edu/>
- [33] C. W. Gao, J. W. Allen, W. H. Green, R. H. West, Reaction mechanism generator: automatic construction of chemical kinetic mechanisms, *Computer Physics Communications* 203 (2016) 212–225.
- [34] N. Cohen, S. W. Benson, Estimation of heats of formation or organic-compounds by additivity methods, *Chemical Reviews* 93 (1993) 2419–2438.
- [35] R. G. Susnow, A. M. Dean, W. H. Green, P. Peczak, L. J. Broadbelt, Rate-based construction of kinetic models for complex systems, *Journal of Physical Chemistry A* 101 (1997) 3731–3740.
- [36] D. G. Goodwin, H. K. Moffat, R. L. Speth, Cantera: An object-oriented software toolkit for chemical kinetics, thermodynamics, and transport processes, version 2.3.0 (2017). URL <http://www.cantera.org>
- [37] R. J. Kee, M. E. Coltrin, P. Glarborg, *Chemically Reacting Flow: Theory and Practice*, 1st Edition, John Wiley & Sons, Hoboken, New Jersey, 2003.
- [38] M. Liu, W. H. Green, Capturing aromaticity in automatic mechanism generation software, *Proceedings of the Combustion Institute* 37 (2017) (submitted).
- [39] K. G. Joback, A unified approach to physical property estimation using multivariate statistical techniques, Sc.M. Thesis, Massachusetts Institute of Technology (1982).
- [40] Advanced Chemistry Development, Inc., ACD/Labs, <http://www.acdlabs.com> (2015).
- [41] M. R. J. Harper, Automated reaction mechanism generation: Data collaboration, heteroatom implementation, and model val-

idation, Ph.D. Thesis, Massachusetts Institute of Technology
(2011).